Search for ferromagnetism in doped semiconductors in the absence of transition metal ions

Erik Nielsen[1,2] and R. N. Bhatt[1,3]
[1]*Department of Electrical Engineering, Princeton University, Princeton, New Jersey 08544-5263, USA*
[2]*Sandia National Laboratories, P.O. Box 5800, Albuquerque, New Mexico 87185, USA*
[3]*Princeton Center for Theoretical Science, Jadwin Hall, Princeton, New Jersey 08544, USA*
(Received 30 July 2010; published 12 November 2010)

In contrast to semiconductors doped with transition metal magnetic elements (e.g., $Ga_{1-x}Mn_xAs$), which become ferromagnetic at temperatures below $\sim 10^2$ K, semiconductors doped with nonmagnetic ions (e.g., silicon doped with phosphorous) have not shown evidence of ferromagnetism down to millikelvin temperatures. This is despite the fact that for low densities the system is expected to be well modeled by the Hubbard model, which is predicted to have a ferromagnetic ground state at $T=0$ on two-dimensional (2D) or three-dimensional bipartite lattices in the limit of strong correlation near half-filling. We examine the impurity band formed by hydrogenic centers in semiconductors at low densities, and show that it is described by a generalized Hubbard model which has, in addition to strong electron-electron interaction and disorder, an intrinsic electron-hole asymmetry. With the help of mean-field methods as well as exact diagonalization of clusters around half filling, we can establish the existence of a ferromagnetic ground state, at least on the nanoscale, which is more robust than that found in the standard Hubbard model. This ferromagnetism is most clearly seen in a regime inaccessible to bulk systems but attainable in quantum dots and 2D heterostructures. If observed, this would be the first experimental realization of a system exhibiting Nagaoka ferromagnetism. We present extensive numerical results for small systems that demonstrate the occurrence of high-spin ground states in both periodic and positionally disordered 2D systems. We examine how properties of real doped semiconductors, such as positional disorder and electron-hole asymmetry, affect the ground state spin of small 2D systems, and use the results to infer properties at longer length scales.

DOI: 10.1103/PhysRevB.82.195117 PACS number(s): 71.10.Fd, 71.27.+a, 71.55.−i, 75.75.−c

I. INTRODUCTION

The utility of introducing impurities into semiconductors can hardly be understated and technology utilizing doped semiconductors is pervasive. One might expect from this that the underlying physics is well understood and while this is true for many aspects of the system there are several mysteries that require further study. This work looks at one of these mysteries: the apparent absence of ferromagnetism in semiconductors that are doped with nonmagnetic elements, at all dopant and carrier densities.

We consider semiconductors with shallow hydrogenic dopants that are randomly positioned within bulk semiconductor. At low dopant densities, such a system can be described by a Hubbard-type model. The Hubbard model on a lattice has two parameters: a hopping amplitude t and an on-site Coulomb repulsion U (see below for details). In the case of half-filling (when the number of electrons is equal to the number of impurities), the Hubbard model can be reduced to a Heisenberg model[1] with an exchange energy that has the correct exponential decay and a prefactor of the correct order of magnitude[2] for hydrogenic systems. Of central importance to this work is that the Hubbard model has a ferromagnetic (FM) ground state for certain parameter ranges. In particular, a rigorous result of Nagaoka[3] shows that a bipartite system with a single hole away from half-filling will have a FM ground state in the strong-correlation limit ($U \gg t$). A mean-field treatment[4,5] corroborates this, and predicts a ferromagnetic phase for small (but finite) deviations from half-filling and large U/t (Fig. 1). Since compensated doped semiconductors are less than half-filled and have tunable U/t (because the hopping parameter varies strongly with dopant density), one might expect them to show FM behavior. However, ferromagnetism is not seen experimentally in compensated semiconductors.[6] One possible cause for this is disorder, coming from the random placement of dopants, since the FM in the Hubbard model is proven only for lattice models. For the half-filled case, randomness in the dopant positions is essential for understanding the magnetism,[7] and the same model works for the compensated case[6] as we discuss later. Blaming the lack of FM entirely on disorder may be premature, however, since disorder does not necessarily destroy FM in other systems. For example, dilute magnetic semiconductors such as $Ga_{1-x}Mn_xAs$, which are even more disordered (with antisite defects and interstitials in addition to the randomness of the dopants), can possess macroscopic FM up to temperatures in excess of 100 K.[8,9] Moreover, in some models disorder may even enhance the ferromagnetic transition temperature.[10,11]

Our study focuses exclusively on semiconductors doped with hydrogenic donors, though is may be generalized to apply to acceptor doped materials as well. For our system, the Hubbard model is particularly appropriate at low densities (i.e., in the insulating phase, where carriers are bound to a few sites and the Coulomb interaction is large compared to the kinetic energy). In this low density limit, each site is treated as an effective hydrogen atom with a corresponding effective Rydberg and Bohr radius

$$\mathrm{Ry}^* = \frac{m^* e^4}{2\epsilon^2 \hbar^2} \quad a_B^* = \epsilon \hbar^2 / m^* e^2, \tag{1}$$

where m^* is the effective mass in the appropriate band and ϵ is the dielectric constant of the host material. In doped semi-

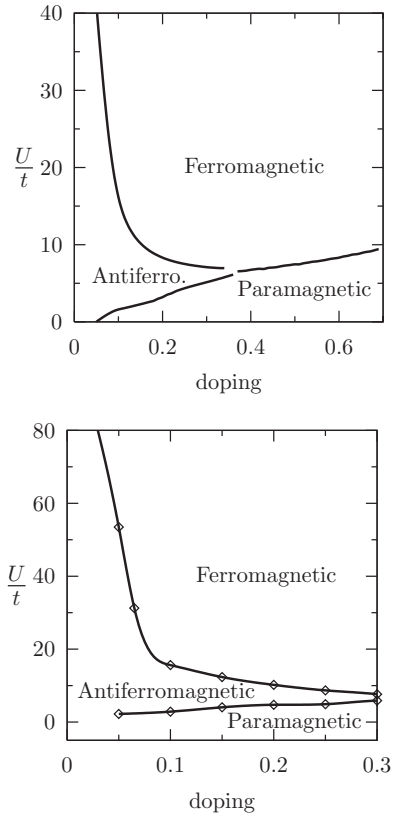

FIG. 1. Zero-temperature mean-field theory phase diagram of the Hubbard model on a 10×10 square lattice (top) and $8\times8\times8$ (512 sites) simple cubic lattice (bottom). Doping (horizontal axis) is defined as the number of extra electrons (above half-filling) per site. Results from Ref. 5, in agreement with Ref. 4.

conductors, typically $\epsilon\sim10-20$ and m^* is 0.05–0.5 times the free electron mass, so that $a_B^*\sim10-500$ Å and $\mathrm{Ry}^*\approx1-50$ meV. Since the Ry^* is usually much smaller than the band gap of the host semiconductor, the lattice lacks low-energy electronic excitations on the energy scale of the impurity electrons and essentially plays the role of an inert vacuum. Realistic effects such as valley degeneracy and mass anisotropy must be included for quantitative calculations but are not essential for the qualitative phenomena of interest to us.[12,13] We will assume that all relevant energy scales are much smaller than the gap between the lowest and higher orbital states on an isolated donor so that we need only care about the $1s$ orbital of each dopant, which consists of two electronic spin-degenerate states at energy denoted E_0. A hydrogenic center, like a hydrogen atom, is known to bind up to two electrons.[14] With a single electron the problem is that of atomic hydrogen (H), and the electron is bound with 1 Ry^*. The two electron case corresponds to the H^- ion, which has a spin singlet ground state bound by 0.0555 Ry^*.[15–17]

Within this "hydrogenic approximation," we seek to better understand why FM is not seen in compensated semiconductors by developing a generalized Hubbard model which is more accurate for the doped semiconductor system. Analyzing this model, we find a *strong* asymmetry in the magnetic behavior of systems doped above and below half-filling; this suggests a way that the effects of disorder may be overcome, and FM observed, in such conventional doped semiconductors.

Throughout this paper, we refer to the phenomenon of ferromagnetism due to kinetic (hopping) terms in the Hamiltonian as "Nagaoka" ferromagnetism, in recognition of Nagaoka's original result, though establishing the true magnetic character of the phase in disordered systems of the type we address requires several further considerations. First, the mean-field treatment of the Hubbard model on the two-dimensional (2D) square and three-dimensional (3D) simple cubic lattices shown in Fig. 1, especially for a disordered structure, are meant as a guide to the physics at short length scales. For the lattice problem, such a treatment does not take into account the possibility of phase separation into carrier rich ferromagnetic and carrier poor antiferromagnetic regions, as has been suggested for 2D.[18] The spatial scale of such a "polaronic" phase may be determined by terms in the Hamiltonian left out of the simple Hubbard Hamiltonian. For the positionally disordered systems we consider, in fact, the precise magnetic structure will be dictated by the disorder; nevertheless, ferromagnetism is possible if clusters on the nanoscale show predominantly large spin ground states (as opposed to singlets), which can percolate at long lengths. Since the basic microscopic mechanism for the occurrence of such a magnetic order (at any length scale nano, meso, or macro) is similar to the one responsible for Nagaoka's original result, we still refer to it as Nagaoka ferromagnetism.

We begin with a review of the Hubbard model and its magnetic properties in Sec. II. We formulate the model Hamiltonian for lattice and disordered systems and focus particularly on conditions and implications of Nagaoka's theorem. However, the Hubbard model in its original formulation neglects an important aspect of a hydrogenic center, namely, that the doubly occupied state is much larger in spatial extent than the singly occupied state. This additional physics, which is a pure correlation effect, is not included in the standard Hubbard model. Adding this to the Hubbard model in Sec. III, results in a generalized Hubbard Hamiltonian appropriate for doped semiconductors. After motivating this model, we compute the magnetic ground state in parameter ranges of interest. We present the results of our model in the following two sections: Sec. IV gives results on small systems (finite lattices, selected symmetric clusters, and small random clusters) while Sec. V considers large systems of random impurities which are divided into smaller, exactly solvable clusters. Finally, Sec. VI highlights our major conclusions and discusses topics for continued work. A short note on the work has appeared previously,[19] and given the extensive study carried out, even the current paper omits some details; interested readers are referred to Ref. 5 for those.

II. BACKGROUND: THE HUBBARD MODEL

This section gives a definition and overview of the Hubbard model originally proposed in the early 1960s (Refs. 20–23) and focus particularly on the Nagaoka's conditions for FM in this model. The Hubbard model combines tight-

binding hopping between nearest neighbors on a lattice with an on-site Coulomb repulsion between electrons in a single orbital state. Though it is one of the simplest interacting models, its on-site correlations are believed to capture the most important source of correlations in solids. Indeed, the Hubbard model displays great diversity of transport and magnetic properties, giving rise to insulating, metallic, and superconducting phases as well as FM, antiferromagnetic (AF), and paramagnetic spin order. It has been used to study a wide range of correlated systems, including Mott-insulator oxides and chalcogenides,[15,24–31] high-T_c superconductors,[32–35] hydrogenic centers in doped semiconductors,[36,37] and quantum dots.[38] Such great interest and applications have resulted in analyses of the model on different lattices,[39,40] with multiple[41] and degenerate[42,43] bands, and with binary alloy disorder.[44] Many studies restrict themselves to the infinite U/t limit,[45,46] which can be realized most effectively in optical lattices,[47] but can be approached in semiconductor systems as well.

The Hamiltonian of the Hubbard model on a *lattice* with N_s sites is given by

$$\mathcal{H} = -t \sum_{\langle i,j\rangle\sigma} (c_{i\sigma}^{\dagger} c_{j\sigma} + \text{H.c.}) + U \sum_{i=1}^{N_s} n_{i\uparrow} n_{i\downarrow}, \tag{2}$$

where i and j range from 1 to N_s, and the first sum is over all distinct nearest-neighbor pairs. Operators $c_{i\sigma}^{\dagger}$ and $c_{i\sigma}$ create and annihilate, respectively, an electron of spin $\sigma \in \{\uparrow, \downarrow\}$ on site i. The parameter t is the quantum mechanical hopping amplitude between (nearest-neighbor) sites, and U is the strength of the on-site Coulomb repulsion. We include a minus sign in front of the kinetic term so that for the familiar example of the tight-binding model with hydrogenic wave functions,[48] $t(r) = 2(1 + r/a_B)\exp(-r/a_B)$ is positive, and restrict ourselves to $U > 0$ (repulsive interaction).

When sites are randomly positioned, a site dependence must be added to the hopping amplitude in Eq. (2). Specifically, t_{ij} is a function of the site separation: $t_{ij} = t(|r_i - r_j|)$ and the resulting Hamiltonian is

$$\mathcal{H}_{rdm} = -\sum_{i<j,\sigma} (t_{ij} c_{i\sigma}^{\dagger} c_{j\sigma} + \text{H.c.}) + U \sum_{i} n_{i\uparrow} n_{i\downarrow} \tag{3}$$

where $i, j = 1, \ldots, N_s$. This accounts for the random positioning of donors found in both uncompensated and compensated *bulk* semiconductors with ≤ 1 electron per donor site (in the latter case, a more rigorous treatment would additionally include random on-site energies reflecting the random fields generated by the positively charged acceptor sites).

In the strong correlation limit $U \gg t_{ij}$ and at half-filling (i.e., one electron per site) the single particle (charge) spectrum has a gap, and the system is insulating [Fig. 2(a)]. The system can have low lying spin excitations and reduces to an effective Heisenberg model.[1] Away from half-filling, where there are carriers [see Fig. 2(b)], one must use a more general low-energy theory that includes a kinetic term called the t-J model[49,50]

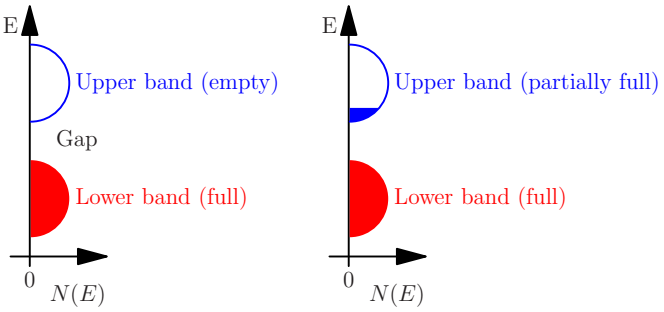

FIG. 2. (Color online) (a) Schematic showing a system at half-filling and (b) slightly above half-filling (b). At half-filling the lower impurity band is completely full and there is a gap to charge excitations. Above half-filling there are electrons present in the upper (unfilled) band that can act as carriers if they occupy extended states (as they do in a lattice). Note also that each band's density of states $N(E)$ is not actually semicircular but drawn this way for convenience.

$$\mathcal{H}_{tJ} = -\sum_{i<j\sigma} t_{ij}((1 - n_{i\bar{\sigma}}) c_{i\sigma}^{\dagger} c_{j\sigma} (1 - n_{j\bar{\sigma}}) + \text{H.c.}) + \sum_{i<j} J_{ij} \left(\vec{S}_i \cdot \vec{S}_j - \frac{1}{4} n_i n_j \right), \tag{4}$$

which operates on the restricted Hilbert space which excludes doubly occupied sites. The AF exchange $J_{ij} = 4t_{ij}^2/U$ and the spin operator $\vec{S}_i$ gives the spin on site i.

For a bipartite lattice at half-filling, the exchange directly gives rise to an antiferromagnet. When the system is above or below half-filling, however, the kinetic term plays a competing role by favoring a ferromagnetic spin configuration. This is so because as carriers hop from site to site they do not disturb an underlying FM spin configuration whereas they necessarily scramble an AF one (see Fig. 3). This scrambling leads to an unfavorable increase in energy and thus the preference for ferromagnetism.[51,52] Relative to an AF state, a FM system with carrier (electron or hole) density δ gains kinetic energy of order $t\delta$ due to carrier delocalization and loses magnetic energy of order is $J = 4t^2/U$. Thus, at a fixed small δ, when U is large enough, $t\delta \gg J$, and the system prefers a FM configuration over the AF one because it allows carriers to be less confined. Understanding the applicability and validity of this argument, and more generally the factors that govern the magnetic competition found in the Hubbard model, has led to several mathematically rigorous results.

Most striking among them is the result of Nagaoka,[3] which states that in the infinite correlation limit $U/t \to \infty$, the Hubbard model on certain finite lattices of dimension $d \geq 2$ with periodic boundary conditions, $t < 0$, and a single hole (away from half-filling), has a FM ground state (i.e., the total spin S^2, where $\vec{S} = \Sigma_i \vec{S}_i$, attains its maximal value). This result, dubbed the Nagaoka theorem, applies to most standard lattices, including the square, simple cubic, triangular, kagomé, bcc, and fcc (hcp).[3,53] In the case of bipartite lattices, such as the square, simple cubic, and bcc, t can be taken positive (the physical sign in the tight binding model) by using electron-hole symmetry of the Hubbard Hamil-

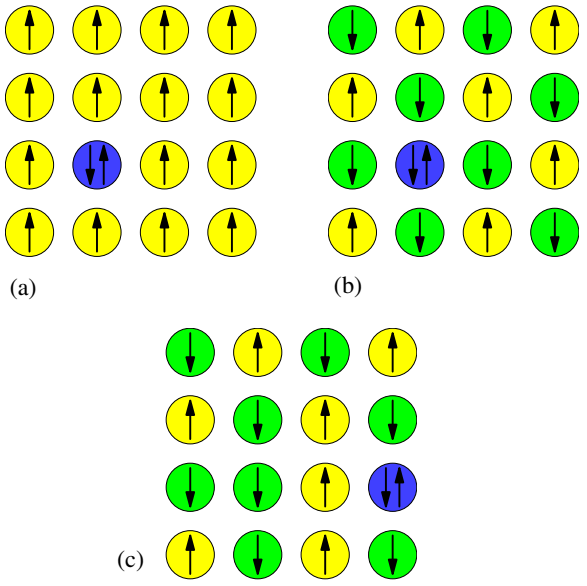

FIG. 3. (Color online) Diagrams showing why the kinetic term favors a ferromagnetic state: in (a) the down spin on the single doubly occupied site can move freely without disturbing the underlying FM background. However, if the background is AF as in (b), motion of electrons on doubly occupied sites scramble the Neel order. Diagram (c) shows the result of the doubly occupied site in (b) moving two sites to the right.

tonian. Along with the rigorous proofs in Nagaoka's and Thouless' work, simpler and more modern mathematical proofs are given by Tian[54] and Tasaki.[55]

Though the stability of the Nagaoka state has been studied extensively and is seen to exist in the Hubbard model, such ferromagnetism has not been observed experimentally. In many Mott-insulator oxides and chalcogenide systems this may be explained by an insufficient U/t to allow for ferromagnetism (and finding a naturally occurring material with large enough U/t seems unlikely). However, in doped semiconductors at low dopant densities, U/t is tunable over several orders of magnitude due to the exponential dependence of the hopping t on the dopant spacing [e.g., $t(r) \sim \exp(-r/a_B)$ in the tight-binding model]. This versatility makes doped semiconductors a promising candidate for Nagaoka ferromagnetism, as it allows U/t to become large ($\sim 100-1000$), achieving for all practical purposes the limit $U/t \to \infty$ required by Nagaoka's theorem. Despite this, the absence of ferromagnetism in experiments on a variety of doped semiconductors, both uncompensated[13,56–59] and compensated,[6] is quite clear. In these experiments, the nearest neighbor coupling, though distributed broadly, had a median value of 1–10 K, and the magnetic susceptibility was searched for down to much lower (mK) temperatures to probe the $T=0$ behavior. The most prominent distinction between the doped semiconductor and the axioms of the Nagaoka theorem is the presence of positional disorder, which thus seems to interfere with ferromagnetic order.

The lack of ferromagnetism in doped semiconductors (whether uncompensated or compensated) can be understood within the framework of the standard Hubbard model with positional disorder [Eqs. (3) and (4)], starting with the half-filled (uncompensated) case. At low densities, $U \gg t_{ij}$, Bhatt and Lee[7] showed, using the disordered Heisenberg model, the low energy physics is very well captured by forming singlets out of strongly coupled pairs of spins in a hierarchical manner, to form what has been variously dubbed a valence-bond glass,[60,61] random singlet,[62] or Bhatt-Lee phase,[63,64] which is quite distinct from the long range antiferromagnetic state on a bipartite lattice. In such a picture, the holes introduced by compensating the system would tend to get localized on one (or a few) valence bonds. Their consequent inability to move long-enough distances precludes any gain in kinetic energy that results from a spin-polarized background hence the lack of any evidence of ferromagnetism from experiments.[6] Thus, even though doped semiconductors give one the ability to tune U/t over several orders of magnitude, Nagaoka ferromagnetism has remained elusive.

III. HUBBARD MODEL FOR HYDROGENIC SYSTEMS

A shortcoming of $\mathcal{H}_{rdm}$ [Eq. (3)] for hydrogenic centers, both for the lattice and random case, is that it does not account for a fundamental property of hydrogen: the two-electron wave function of the H^- ion has much greater extent than the one-electron wave function of the H atom. This is reflected in the binding energy of H^- being only 0.0555 Ry^*, which has been well substantiated for hydrogenic centers in semiconductors[65–67] whereas 1 Ry^* is necessary to remove the electron of H.[15,16] Indeed, using that an effective Bohr radius a^* scales as $1/\sqrt{E_{\mathrm{binding}}}$, we find that the ratio of Bohr radii for H^- and H, $a^*_{H^-}/a^*_H = \sqrt{1.0}/\sqrt{0.0555} \approx 4$, showing that the wave function of H^- is several times larger than that of H. Variational treatments of the H^- ion,[16] as well as an effective pseudopotential calculation,[68] determine the ratio to be in the range 2–4. This large ratio is consistent with the observation of charge-transfer excitations in the far infrared spectra of donor pairs.[12,69] This affects the Hubbard description of the system because it is much easier for an electron on a doubly occupied hydrogenic center to hop away than it is for the electron on a singly occupied site to make a similar hop. This implies that the hopping amplitude seen by an itinerant electron, hopping around in a background of singly occupied sites, is larger than that seen by a hole in a similar background. The fact that the ratio of the two radii is substantial (2–4), and the hopping amplitude is exponentially dependent on the radius (in the low-density regime), suggest that a doped semiconductor above half-filling is in a quite different regime of parameters than the conventional compensated semiconductor (a system below half-filling). Such a regime, while not obtainable in bulk doped semiconductors, should be realizable in semiconductor heterostructures, as well as quantum dots. In Hubbard model parlance, near half-filling the hopping amplitude for an electron is much larger than for a hole. At the very least, the different radii of the doubly vs singly occupied sites suggest that we modify lattice Hubbard Hamiltonian (2) to become

$$\mathcal{H}^* = -\sum_{\langle i,j\rangle\sigma} (t_{ij}(n_i,n_j)c^\dagger_{i\sigma}c_{j\sigma} + \mathrm{H.c.}) + U\sum_i n_{i\uparrow}n_{i\downarrow}, \quad (5)$$

where n_i is the total occupation of site i and the hopping now has occupation dependence given by the piecewise function

(the hopping corresponding to the different amplitudes t and $\tilde{t}$ is shown pictorially on the right)

$$t(n_i,n_j)=\begin{cases}\tilde{t} & n_j=1,n_i=2\\ t & \text{otherwise}\end{cases}, \quad (6)$$

where $\tilde{t}$ is larger (and as we will see, can be much larger) than t.[19] In Eq. (6), there is also the dependence of $\tilde{t}$ and t on i and j, which we have omitted to show explicitly. This model enhances the hopping from a doubly occupied site to an already singly occupied site (which will become doubly occupied after the hop). One may question why the hopping from a doubly occupied site to an empty site [the middle picture of Eq. (6)] is not also enhanced. The primary reason is that the present formulation is the only way, within the single-band Hubbard model, to preserve the asymptotic spatial dependence of the effective exchange interaction: $J(r) \sim e^{-2r/a_B^*}$ (recall $J \sim t^2/U$ and $t \sim e^{-r/a_B^*}$). This is of essential importance since this relation for J has been shown to be asymptotically exact.[70] In the disordered case, Eq. (5) becomes

$$\mathcal{H}_{rdm}^* = -\sum_{i,j,\sigma}(t_{ij}(n_i,n_j)c_{i\sigma}^\dagger c_{j\sigma}+\text{H.c.})+U\sum_i n_{i\uparrow}n_{i\downarrow}, \quad (7)$$

where $t_{ij}(n_i,n_j)=\tilde{t}_{ij}$ when $n_j=1$ and $n_i=2$ and otherwise $t_{ij}(n_i,n_j)=t_{ij}$. Note that Eq. (5) is in general *not* electron-hole symmetric (Only when $\tilde{t}=t$ and the system is on a bipartite lattice is electron-hole symmetry preserved.[71]). Hirsch has investigated a similar Hubbard model with occupation-dependent hopping but in a different regime with its focus on superconducting pairing.[72]

This asymmetry is clearly seen in the low-energy theories, where above half-filling Eq. (5) reduces to a $\tilde{t}$-J model

$$\mathcal{H}_{tJ} = -\sum_{\langle ij\rangle\sigma}\tilde{t}_{ij}[(1-n_{i\bar{\sigma}})c_{i\sigma}^\dagger c_{j\sigma}(1-n_{j\bar{\sigma}})+\text{H.c.}] + \sum_{\langle ij\rangle}J_{ij}\left(\vec{S}_i\cdot\vec{S}_j-\frac{1}{4}n_in_j\right) \quad (8)$$

whereas below half-filling the effective low-energy model is the t-J model ($\tilde{t}$ replaced by t).

It is important to remember that the electron creation and annihilation operators in these models act on a system with a fixed number and arrangement of sites. In a semiconductor, each site corresponds to a dopant atom and when we speak of adding electrons or holes to the system we mean addition or subtraction of carriers while *leaving the underlying dopant configuration fixed*. Thus, the electron-hole asymmetry here is *not* an asymmetry between n-type and p-type semiconductors but an asymmetry between a doped semiconductor which has more electrons than dopant atoms and one which has less electrons dopant atoms.

One way to view the manifest electron-hole asymmetry of models in Eqs. (5) and (7) is that systems above half-filling are effectively *less random*, and hold greater hope for the Nagaoka phenomenon to take place. This reasoning follows from electrons having more extended wave functions than holes and the concomitant existence of two distinct length scales. Because the electron wave functions average over much more of the disorder, systems with a small percentage of extra electrons experience a greatly reduced effect of the positional disorder when compared with corresponding hole-doped (i.e., compensated) systems and so behave more like the uniform lattice. The large difference of length scales between the carrier (hole) wave function's Bohr radius and the d-electron wave function of a Mn dopant in GaAs is crucial for the ferromagnetism in the diluted magnetic semiconductor $Ga_{1-x}Mn_xAs$.

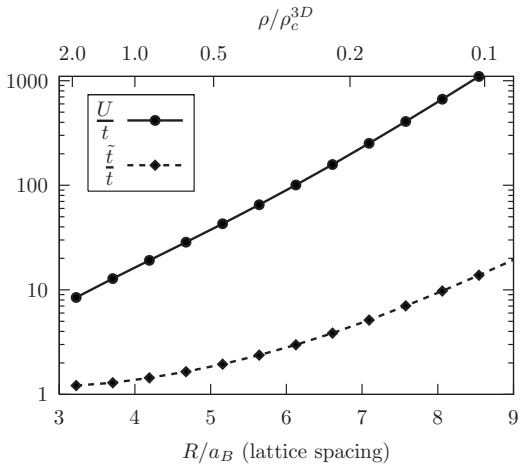

FIG. 4. Variation in ratios U/t and $\tilde{t}/t$ with the dopant spacing (related to the dopant density ρ by $\rho=\frac{1}{R^3}$ so the metal-insulator occurs at $R_c/a_B=4$).

To find values of U/t and $\tilde{t}/t$ appropriate for doped semiconductors, upper and lower impurity bands were calculated for donors placed on a simple cubic lattice for a spin-polarized configuration. We follow Bhatt and Rice,[17] and use pseudopotentials and a sphericalized Wigner-Seitz method on a (cubic) superlattice. Details of the band calculation can be found elsewhere.[17,68] We extract the dependence of t and $\tilde{t}$ on the impurity density (or equivalently, on the lattice constant) by fitting the calculated bandwidths to a tight-binding model using the relationship $2zt=W$, where t is the hopping parameter, W is the bandwidth, and z is the lattice coordination number. The upper band is used to give $\tilde{t}$ and the lower band t. U is given by the gap between the bands at zero density, which we find to be approximately 1 Ry^*. Figure 4 shows the dependence of the dimensionless Hubbard parameter ratios on the superlattice spacing (lower axis) and impurity density (upper axis). It shows clearly that the range of U/t and $\tilde{t}/t$ can be varied substantially in the doped semiconductors. The large span of U/t has its origin in the exponential dependence of the hopping parameter on the atomic spacing, and the variation in $\tilde{t}/t$ from the relatively large size of the two-electron wave function appearing as a factor in this exponential.

In the results that follow, we either use the exact parameter ratios found here or consider the effect of varying the parameter ratios within the ranges $U/t=[5,100]$ and $\tilde{t}/t=[1,10]$, which are conservative when compared to the physically attainable ranges.

IV. RESULTS FOR GROUND STATE SPIN IN FINITE SYSTEMS

In this section we present the results of diagonalizing the Hubbard Hamiltonians (5) and (7) for finite systems. The results and discussion are divided into units based on the amount of structure present in the system, and what types of boundary conditions were used. In Sec. IV A–IV C, the kinetic (hopping) amplitudes $(t,\tilde{t})$ are simply the treated as parameters, whereas in Sec. IV D, which studies ensembles of random clusters, they are taken to be specific functions of the distances between sites. Section IV A considers systems with finite lattice structure and periodic boundary conditions. Only nearest-neighbor links are kept in the model [see Eq. (5)] so that there is a single pair $(t,\tilde{t})$ of kinetic parameters. We refer to a lattice as being bipartite or nonbipartite if the corresponding Hubbard model with only nearest-neighbor hopping is, respectively, bipartite or not. Section IV B presents results from clusters with open boundary conditions and selected structures for which all nearest neighbors are equidistant (so there is again a single pair of kinetic parameters). We use the term *cluster* to refer to a finite system possessing less symmetry than a finite lattice. In Sec. IV C, clusters constructed to have only two or three pairs of kinetic parameters are considered with open boundary conditions. Finally, in Sec. IV D we analyze ensembles of random clusters. We generate these ensembles with a fixed density and exact diagonalization results of the individual clusters are averaged to produce our final results.

A. Finite lattices

We have solved the nearest-neighbor Hubbard and corresponding $\tilde{t}$-J models on finite square (8, 10, and 16 sites), honeycomb (6 and 10 sites), and triangular (7 and 9 sites) lattices. Choice of the unit cell in the former two bipartite structures allows a classical Neel state spin assignment, which is important since a finite bipartite lattice that is magnetically frustrated due to boundary conditions may have an exaggerated preference for FM.

Each finite lattice is given periodic boundary conditions and doped with up to two electrons or holes away from half-filling. Denoting the number of sites by N_s and electrons by N_e, this means that $N_s-2\leq N_e\leq N_s+2$. The Hubbard model depends on the two dimensionless ratios U/t and $\tilde{t}/t$, whereas the $\tilde{t}$-J model depends only on $\tilde{t}/J=\frac{1}{4}(\tilde{t}/t)(U/t)$. Thus, the value of $\tilde{t}/J$ marking the onset of the Nagaoka state defines a straight line in log U/t vs log $\tilde{t}/t$ space with slope -1. We consider each lattice in turn below.

1. Square lattice

Figure 5 shows the ground-state spin phase diagram for the 8-, 10-, and 16-site square lattices doped with one electron, up to $\tilde{t}/t=5$. One sees that an increase in $\tilde{t}/t$ causes the region where the ground state attains its maximum spin to increase. This confirms that a FM ground state is more likely when the carriers (an extra electron in this case) have greater hopping amplitude. Up to $\tilde{t}/t=5$, the minimal U/t needed for a fully polarized ground state falls roughly as a power law

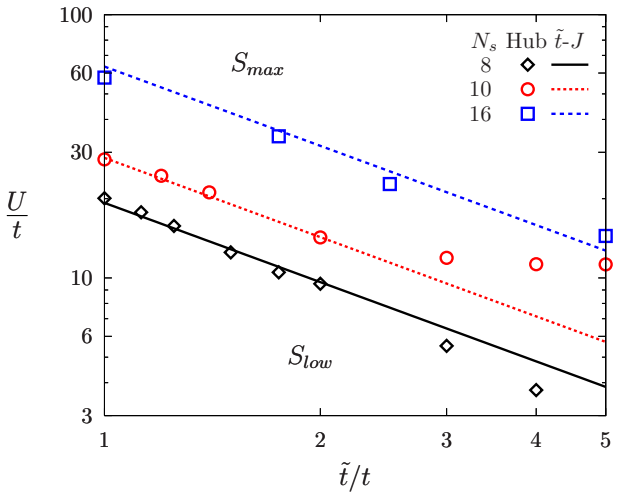

FIG. 5. (Color online) Ground-state spin diagram resulting from the exact diagonalization of Eq. (5) on 8-,10-, and 16-site square lattices (periodic b.c.) with 9, 11, and 17 electrons respectively. Hubbard model results are displayed as open symbols. Lines show the result of the corresponding $\tilde{t}$-J model as described in the text. S_{max} denotes the region of largest allowed spin (actual value depends on the lattice size) and S_{low} marks the region of unsaturated (usually minimal) ground state spin.

with $\tilde{t}/t$. The $\tilde{t}$-J model gives a fairly accurate fit to the Hubbard data (predicting a power law with exponent -1, shown by the lines in Fig. 5). The fit is especially good at low $\tilde{t}/t$, which coincides with larger U/t values and thus is where we expect the $\tilde{t}$-J model to be most accurate.

A comparison of these electron-doped systems with corresponding hole-doped systems reveals a pronounced electron-hole asymmetry. This is expected from the model, since for $\tilde{t}\neq t$ the Hamiltonian is not electron-hole symmetric: electrons hop with $\tilde{t}$ whereas holes hop with amplitude t. Figure 6 compares the Hubbard model with $N_e=N_s\pm 1$ (one extra electron or one hole) on finite square lattices. In the larger 10- and 16-site lattices with one hole we see very little dependence of the ground-state spin on $\tilde{t}/t$, as would be na-

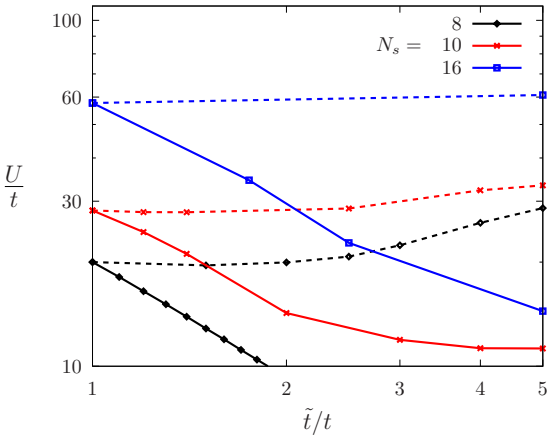

FIG. 6. (Color online) Ground-state spin diagram for the 8-, 10-, and 16-site square lattices showing the asymmetry between doping with a single hole (dashed line) and a single electron (solid line).

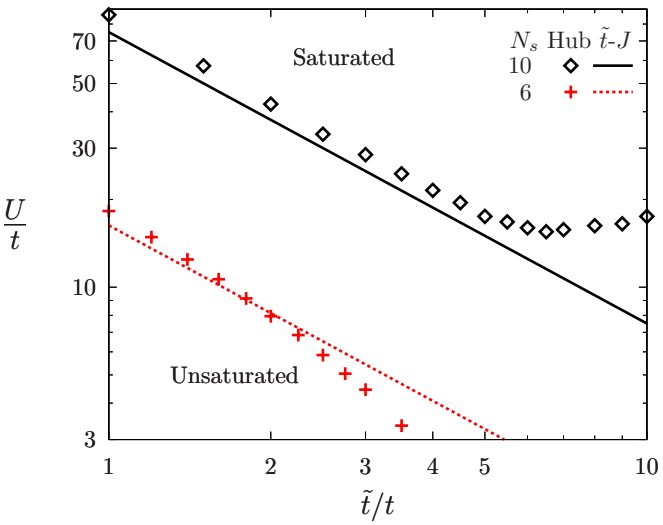

FIG. 7. (Color online) Ground-state spin diagram from the exact diagonalization of 6- and 10-site honeycomb lattices doped with a single electron (i.e., with seven and 11 electrons, respectively) showing the boundary of the region where there is a complete spin polarization. In the 6-site lattice the transition is from $S=5/2$ to $S=3/2$ whereas in the 10-site lattice the transition is more abrupt, changing from $S=9/2$ to $S=1/2$ within the resolution used.

ively expected. It is clear that the asymmetry between the electron- and hole-doped results originates from the electronic states having greater radius than the hole states since for equal radii ($\tilde{t}=t$) the square lattice is bipartite and the problem is electron-hole symmetric. Figure 6 is the first of many cases where high-spin ground states are attained at *much* lower U/t in the electron-doped case than in the hole-doped case.

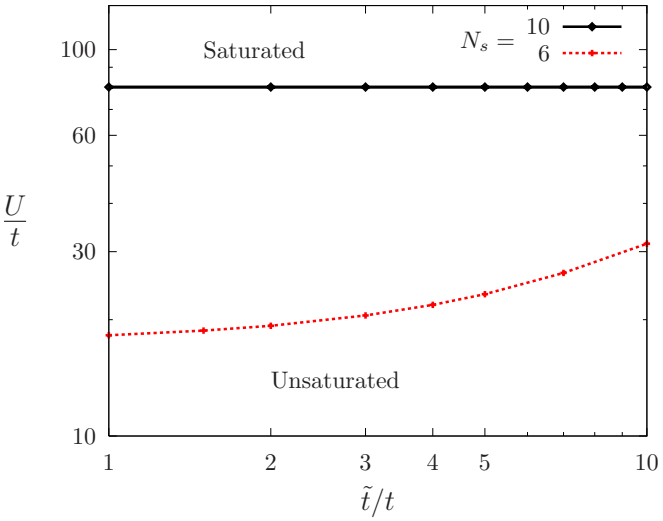

FIG. 8. (Color online) Exact diagonalization results showing the boundary of the fully spin-polarized region on the 6- and 10-site honeycomb lattices doped with a single hole (i.e., with five and nine electrons, respectively). In the 10-site case, the spin on the unsaturated side of the transition is $S=\frac{1}{2}$ except for a region of $S=\frac{5}{2}$ found at intermediate U/t for $\tilde{t}/t>10$; on the 6-site lattice the unsaturated state has uniform spin $\frac{3}{2}$. Note that there is much less variation with respect to $\tilde{t}/t$ when compared with Fig. 7.

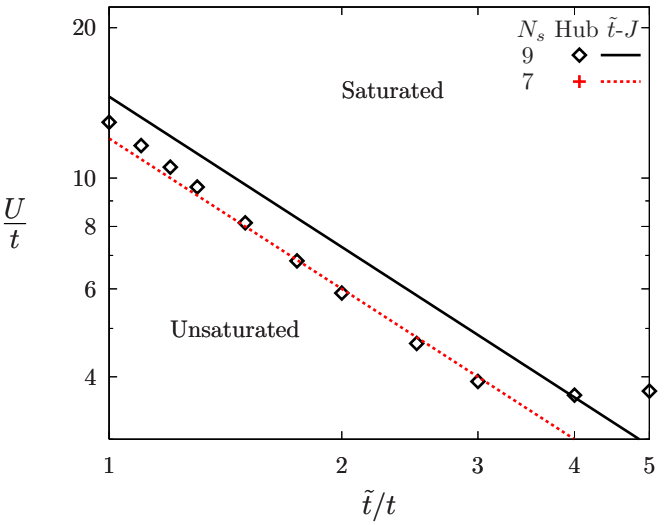

FIG. 9. (Color online) Ground-state spin diagram from the exact diagonalization of 7- and 9-site triangular lattices when doped with a single electron, showing the region of saturated spin. On the 9-site lattice, the unsaturated region is predominantly $S=0$ except for a sliver of $S=2$ close to the transition. There is no transition on the Hubbard 7-site lattice, which has a maximally polarized ground state ($S=3$) for the entire plotted area. In the corresponding t-J model, however, the 7-site lattice has a transition from $S=3$ to $S=2$ near $\tilde{t}/J\approx 3.0$ (shown by the dotted line).

2. Honeycomb lattice

The honeycomb lattice is bipartite and thus the Hubbard model is electron-hole symmetric on it for $\tilde{t}=t$. The mean-field ground-state phase diagram of the $\tilde{t}=t$ Hubbard model for hole-doped systems shows the existence and stability of the Nagaoka phase at large U/t near half-filling.[73] The magnetic ground-state diagrams for Hamiltonian (5) on 6- and 10-site honeycomb lattices with one electron or hole away from half-filling ($N_e=N_s\pm 1$) are shown in Figs. 7 and 8, respectively.

We find similar qualitative behavior to that of the square lattices: for systems with $N_e=N_s+1$, increasing $\tilde{t}/t$ expands the region of phase space for which the spin is maximal. Again, the $\tilde{t}$-J model result agrees well with the Hubbard results for low $\tilde{t}/t$. In the case of single hole-doping ($N_e=N_s-1$), there is little dependence on $\tilde{t}/t$ in the 10-site lattice whereas there is the opposite $\tilde{t}/t$ dependence in the smaller 6-site lattice, similar to the case of the 8-site square lattice.

3. Triangular lattice

The triangular lattice is a Bravais lattice of particular interest since it magnetically frustrated (not bipartite). A recent study of the triangular lattice[74] using a many-body expansion technique finds that, at large U/t, a 120°-ordered AF phase is stable at and below half-filling, and becomes unstable above half-filling. In past studies of finite clusters, it was likewise found that at half-filling antiferromagnetic states are optimal in nonbipartite systems (due to the quantum fluctuations arising from what would be frustrated bonds in a static picture).[75]

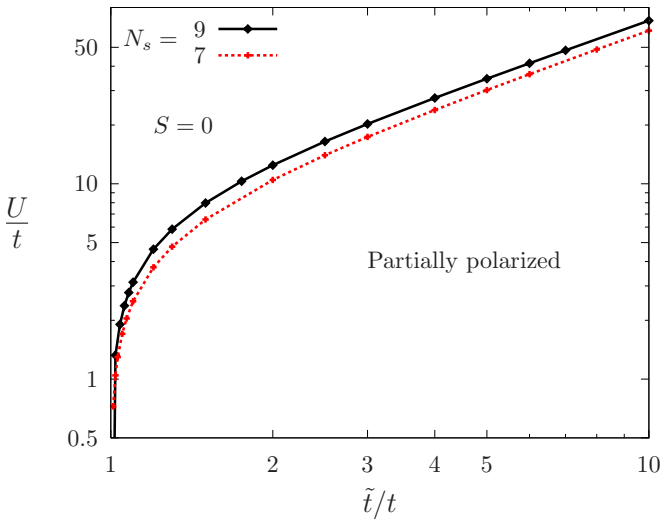

FIG. 10. (Color online) Ground-state spin diagram for the 7- and 9-site triangular lattices doped with a single hole. Nowhere is the ground-state spin saturated. Instead, there is a region of minimal spin ($S=0$) at large U/t which is encroached upon by a region of partial spin polarization ($S=2$ and $S=3$ for 7- and 9-sites, respectively) as $\tilde{t}/t$ increases.

With a single extra electron ($N_e=N_s+1$), the Hubbard model on 7- and 9-site lattices displays saturated ferromagnetism very strongly (on the 9-site lattice with $\tilde{t}=t$, $U/t \approx 15$ results in a spin-polarized ground state). Figure 9 shows our results for the Hubbard model on finite triangular lattices with one extra electron. Classically, the observed dominance of ferromagnetism could be linked to a suppression of competing AF configurations (frustrated on the triangular lattice). One must be careful, however, when applying this reasoning to quantum models, as studies have shown that antiferromagnetism is *enhanced* on the triangular lattice with a single hole[76] due to the subtle interplay of quantum phases. The regnancy of ferromagnetism may also be due to the large number of tight loops in the lattice. Pastor *et al.*[77] have remarked that the presence of triangular or square loops coincides with ferromagnetism in finite clusters and we reach similar findings in our study of clusters below (see Secs. IV B and IV C). The strong FM we see here suggests that this connection extends to lattices as well.

The $\tilde{t}$-J data for the triangular lattice fits the Hubbard data less well than in the previous bipartite lattices. For the 9-site triangular lattice the $\tilde{t}$-J result underestimates the region of saturated spin, and in the case of the 7-site triangular lattice, the Hubbard model does not even transition to the unsaturated state predicted by the $\tilde{t}$-J model. The discrepancy is not surprising, given the low U/t values at which the transitions occur.

Since the triangular lattice problem is not bipartite, there can be (and is) electron-hole asymmetry even when $\tilde{t}=t$. Figure 10 shows the ground state phase diagram for single hole-doped 7- and 9-site triangular lattices ($N_e=N_s-1$). These plots are qualitatively different from those of the hole-doped square and honeycomb lattices: the high-spin region is unsaturated and lies at *lower* U/t than a minimal-spin region which dominates at large U/t. As $\tilde{t}/t$ is increased, the partially polarized region expands up to larger U/t values. The mechanism for this may be related to the "kinetic antiferromagnetism" studied by Haerter and Shastry,[76] which explains how the phase dependence of a single hole's motion enhances antiferromagnetism.

#	Geometry	S^{2h}_{max}	S^{1h}_{max}	S^{1e}_{max}	S^{2e}_{max}
1		-	$\frac{1}{2}$	$\frac{1}{2}$	-
2		$\frac{1}{2}$	0	1	$\frac{1}{2}$
3		0	$\frac{3}{2}$	$\frac{3}{2}$	0
4	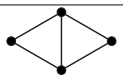	0	$\frac{1}{2}$	$\frac{3}{2}$	1
5		$\frac{3}{2}$	1	0	$\frac{1}{2}$
6	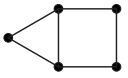	$\frac{1}{2}$	1	2	$\frac{1}{2}$
7	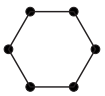	1	$\frac{1}{2}$	$\frac{1}{2}$	1
8	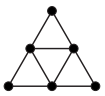	1	$\frac{3}{2}$	$\frac{5}{2}$	0
9	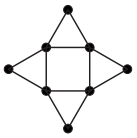	2	$\frac{3}{2}$	$\frac{5}{2}$	1

FIG. 11. Summary of clusters that have a single pair of hopping parameters. $S^x_{\max}$ is the maximum spin obtained in the window $\tilde{t}/t \in [1,10]$, $U/t \in [5,100]$ when the system has one or two holes or electrons away from half-filling ($x=1h,2h,1e,2e$, respectively). Note the correspondence of high-spin states with larger numbers of tight loops.

B. Selected symmetric clusters

Next we consider a select group of two-dimensional Hubbard clusters that, such as the finite lattices, have only a single pair of hopping amplitudes, t and $\tilde{t}$. These clusters are given *open* boundary conditions, which corresponds to a small number of sites (dopants or quantum dots) positioned in a plane such that every pair of nearest neighbors is equidistant. We calculate the phase diagram for $1 \leq \tilde{t}/t \leq 10$ and $5 < U/t < 100$ when doped with one or two electrons away from half-filling (in either direction). Figure 11 summarizes the results, giving each cluster's geometric structure and its maximal spin as a function of doping. We see that in most cases, the highest spin is attained when doped with a single electron, following our expectation that a low density of ex-

$\#_{cl}$	Geometry	S^{2h}_{max}	S^{1h}_{max}	S^{1e}_{max}	S^{2e}_{max}
1		$\frac{1}{2}$	0	1	$\frac{1}{2}$
2		0	$\frac{1}{2}$	$\frac{3}{2}$	1
3	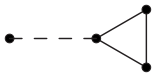	0	$\frac{1}{2}$	$\frac{1}{2}$	1
4		$\frac{1}{2}$	1	2	$\frac{1}{2}$
5		$\frac{1}{2}$	1	1	$\frac{1}{2}$
6	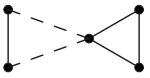	$\frac{1}{2}$	1	1	$\frac{1}{2}$
7	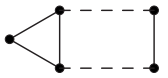	$\frac{1}{2}$	1	2	$\frac{1}{2}$
8		$\frac{1}{2}$	1	0	$\frac{3}{2}$
9		1	$\frac{1}{2}$	$\frac{1}{2}$	1
10	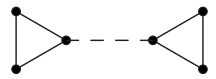	1	$\frac{1}{2}$	$\frac{3}{2}$	0
11	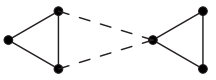	1	$\frac{3}{2}$	$\frac{3}{2}$	2
12		0	$\frac{1}{2}$	$\frac{5}{2}$	0
13	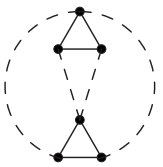	1	$\frac{3}{2}$	$\frac{5}{2}$	0

$\#_{cl}$	Geometry	S^{2h}_{max}	S^{1h}_{max}	S^{1e}_{max}	S^{2e}_{max}
14	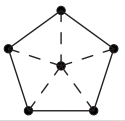	1	$\frac{3}{2}$	$\frac{5}{2}$	1
15	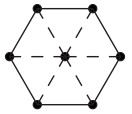	$\frac{1}{2}$	0	3	$\frac{3}{2}$
16		$\frac{1}{2}$	0	1	$\frac{1}{2}$
17	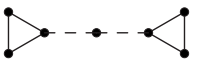	$\frac{1}{2}$	1	1	$\frac{3}{2}$
18	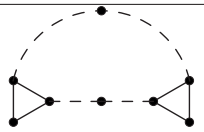	1	$\frac{1}{2}$	$\frac{7}{2}$	2
19		1	$\frac{1}{2}$	$\frac{3}{2}$	0
20	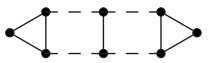	1	$\frac{3}{2}$	$\frac{7}{2}$	3
21	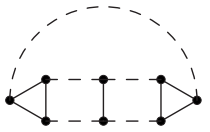	1	$\frac{1}{2}$	$\frac{7}{2}$	3
22	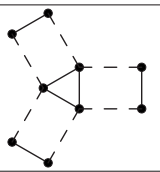	-	-	4	-
23	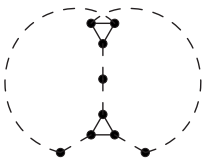	$\frac{3}{2}$	1	2	$\frac{5}{2}$

FIG. 12. Summary of maximum ground-state spins for clusters that have two pairs of kinetic parameters (two distinct nearest-neighbor distances). Solid lines represent hopping amplitude t_1 and dashed lines t_2. Cluster geometries are listed by size, and maximal spin is given for dopings of -2, -1, 1, and 2 electrons away from half-filling. Each cluster is identified by a number, $\#_{cl}$, and the maximum is taken over the region $t_2/t_1 \in [1,10]$, $t_1/U \in [0.01,0.5]$ for $\tilde{t}_i/t_i$ uniformly set=1, 5, and 10.

tra electrons will favor spin polarization. Clusters 1–4, 6, and 7, attain their *maximal* ground state spin when doped with one electron. In contrast, clusters 5 and 9 have greater spin polarization below half-filling when doped with two holes. For a detailed discussion of the results, the reader is referred to Ref. 5.

C. Distorted clusters

More complex 2D clusters are obtained by allowing more than one pair of hopping parameters (i.e., hopping is allowed between sites of different separation distances). Here we consider clusters with two and three pairs of distinct hopping parameters $\{(t_i,\tilde{t}_i): i \in (1,2,3)\}$. Some of these can be viewed as geometric perturbations of clusters in the last section while many are new geometries not possible under the restriction of equidistant nearest neighbors. For a select group of clusters with two pairs of hopping parameters, we consider the ground state spin as a function of t_2/t_1 and U/t_1 at a uniform fixed $\tilde{t}_i/t_i$, $i=1,2$. Our analysis is done over the substantial region of phase space: $t_2/t_1 \in [1,10]$, $t_1/U \in [0.01,0.5]$. (Note that this extends to $U/t<10$, outside the physical range found earlier, but in the direction that favors non-ferromagnetic behavior.) The results are summarized in

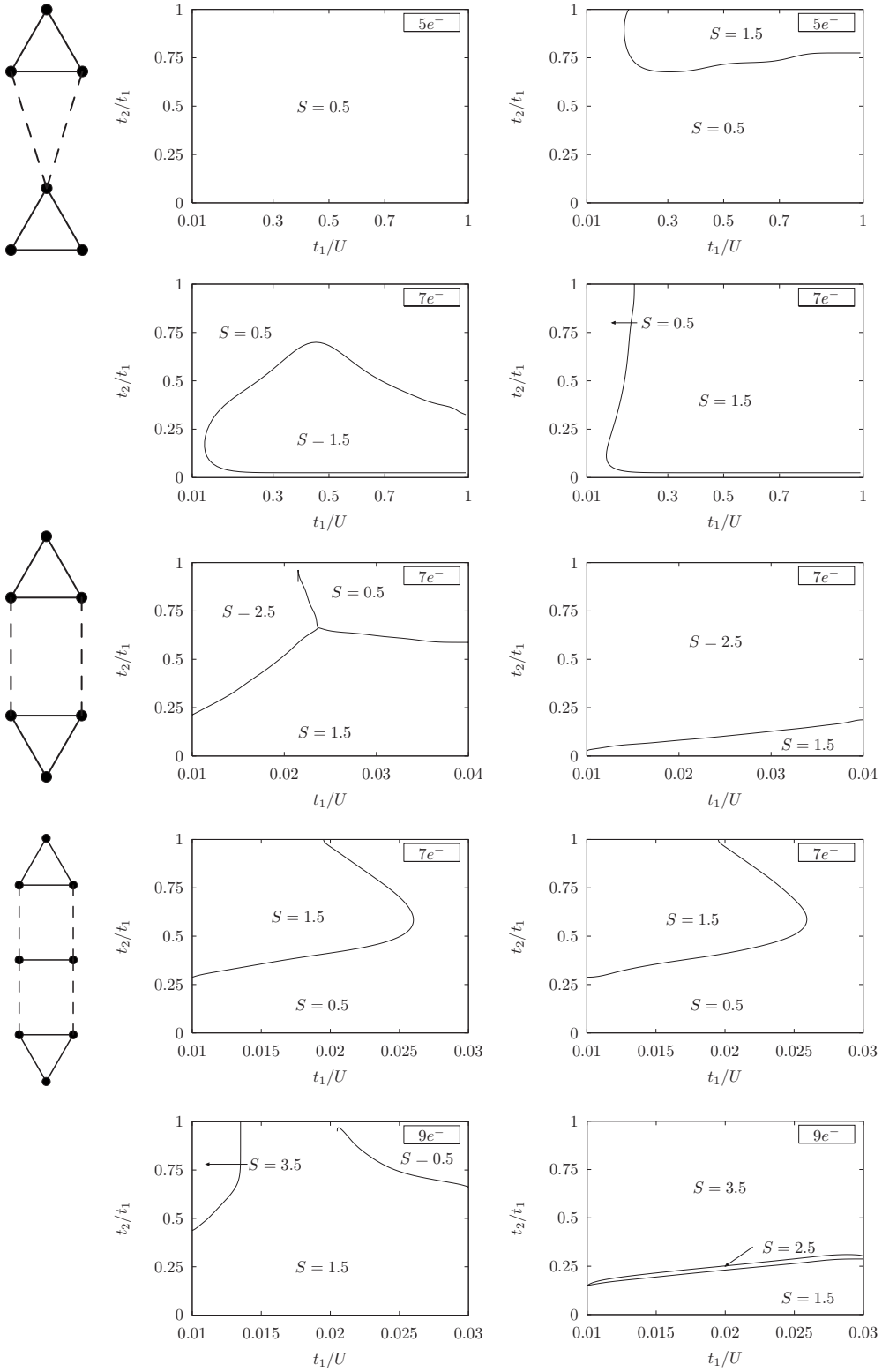

FIG. 13. Ground-state spin diagrams for selected clusters from Fig. 12.

Fig. 12, which show, for each of 23 different geometries, the maximal spin achieved with a doping of up to two electrons or holes (the maximum is taken over the region of phase space stated above). Again we find that most clusters attain their highest spin when doped with $1e^-$ (clusters 1, 2, 4, 7, 10, 12, 14, 15, 18, 20, and 22). Some of the larger clusters also have high spins when doped with two electrons (clusters 11, 18, 20, and 23), since their density is still low enough to favor FM. Although in most cases the maximal spin is greater for electron doping than hole doping, there are some which attain high spins even when hole doped (e.g., clusters 8, 9, 11, and 15).

We focus on the ground-state spin behavior of three clusters from Figs. 12: 11, 12, and 20. Ground state phase diagrams showing the spin for these clusters are in the Fig. 13. Each row of the table shows the geometry and two ground-state phase diagrams of a cluster with a fixed number of sites N_s and electrons N_e. The two diagrams correspond to $\tilde{t}/t=1$ and 5, as indicated by the column headings. The charge of the cluster $Q=N_s-N_e$ (the negative of its doping relative to half-filling) is given in the third column. For each selected cluster, phase diagrams are only shown for $Q=\pm 1$. $Q=+1$ corresponds to hole doping, $Q=-1$ to electron doping. The hole-doped case is not shown for cluster 12 since it is trivial ($S=0.5$ everywhere). The transition lines in these plots are found by finding the ground state spin on a grid in parameter space, then fitting the transitions between grid points with smooth curves. Detailed phase diagrams of *all* nontrivial cases are given Ref. 5.

Several conclusions may be drawn from this data. First, there are many instances of high-spin ground states among these clusters, many of which can be thought of as a weak coupling (t_2) between triangles and pairs with a stronger internal coupling (t_1). In a real system, where the broad distribution of intersite distances due to positional randomness creates exponentially strong and weak bonds, these results give some hope that the spin polarization seen in the isolated triangle, for example, will survive in the presence of perturbation due to other sites and that this interaction may even lead to spin polarization on longer length scales. Second, it is found almost universally that increasing $\tilde{t}/t$ leads to greater spin polarization in *electron-doped* clusters, just as in the finite lattices (Sec. IV A) and single-hopping parameter clusters (Sec. IV B). In electron-doped clusters, we continue to see a correlation between the number of triangular loops in a cluster and that cluster's maximal spin. For instance, if we compare clusters 5 and 7 with clusters 14 and 15 of Fig. 12, we find the latter are much more magnetic. In hole-doped systems we generally find lower spin values, and often there is a high-spin region at *low* U/t_1. This inverted relationship in clusters below half-filling was also found in Sec. IV B and on the 8-site square lattice. Lastly, we note that although there is potential for high-spin states, there are many clusters that have large regions of minimal ground state spin. We find overall that the Nagaoka-type ferromagnetic effect we observe is very sensitive to geometry, though the sensitivity decreases at large $\tilde{t}/t$.

D. Randomly distributed finite clusters of fixed density

In Secs. IV B and IV C, we solved generalized Hubbard and $\tilde{t}$-J models on a variety of clusters that were constructed to have some spatial symmetries and at most two pairs of hopping parameters $(t_i,\tilde{t}_i)$. This section and the next give an analysis of clusters with completely random structures. Also, instead of considering just a range of $\tilde{t}/t$ values, to be representative of actual doped semiconductors we use the tight-binding parameters given by a fit to the band calculation outlined at the end of Sec. III. In d dimensions, clusters with N_s sites and fixed density ρ are generated by randomly placing N_s sites within a d-dimensional hypercube of side length

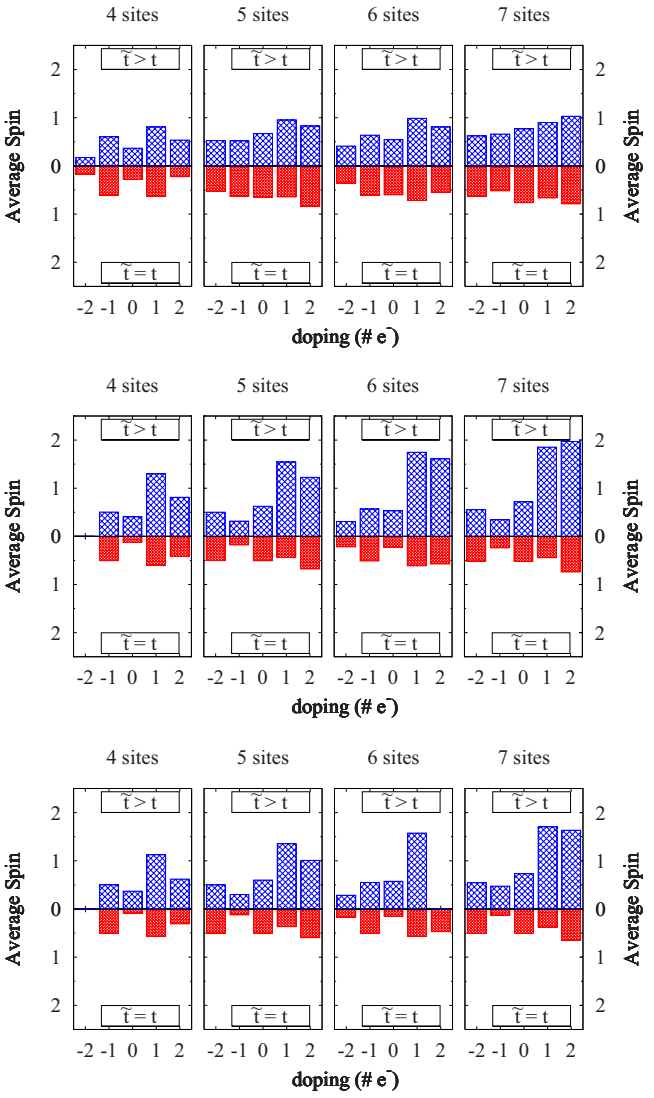

FIG. 14. (Color online) Ground-state average spin of 2D random clusters with fixed size and density, and *open boundary conditions*, as a function of electron-doping (negative=hole doping). The lower half of plots are the result of setting $\tilde{t}_{ij}=t_{ij}$, determined by the bandwidth of the lower Hubbard band. The upper half use $\tilde{t}_{ij}$ determined by the bandwidth of the upper Hubbard (D^-) band.

L such that $\rho(a_B^*)^{-d}=N_s/L^d$. We fix $U=1$ Ry* and determine the hopping parameters by setting $t_{ij}=t(|\vec{r}_i-\vec{r}_j|)$ and $\tilde{t}_{ij}=\tilde{t}(|\vec{r}_i-\vec{r}_j|)$. Functions $t(r)$ and $\tilde{t}(r)$ are given by the lattice calculation described earlier (see Fig. 4) and together take into account the larger extent of the D^- state.

Given a fixed cluster size and density, we exactly solve many (between 10^4 and 10^6) clusters. Results are calculated for clusters in two and three dimensions with sizes from $N_s=4-7$ and for densities $\rho=\frac{1}{1600}$, $\frac{1}{160}$, and $\frac{3}{160}$ in 2D, (corresponding to $\approx$0.005, 0.05, and 0.15 times the Mott metal-insulator transition density) and $\rho=\frac{1}{6400}$, $\frac{1}{640}$, and $\frac{3}{640}$ in 3D (corresponding to 0.01, 0.1, and 0.3 times the Mott density). We present results for systems in 2D and 3D systems with open boundary conditions here (results for periodic boundary conditions in both 2D and 3D are given in Ref. 5, and are qualitatively similar). In an actual macroscopic sample, clus-

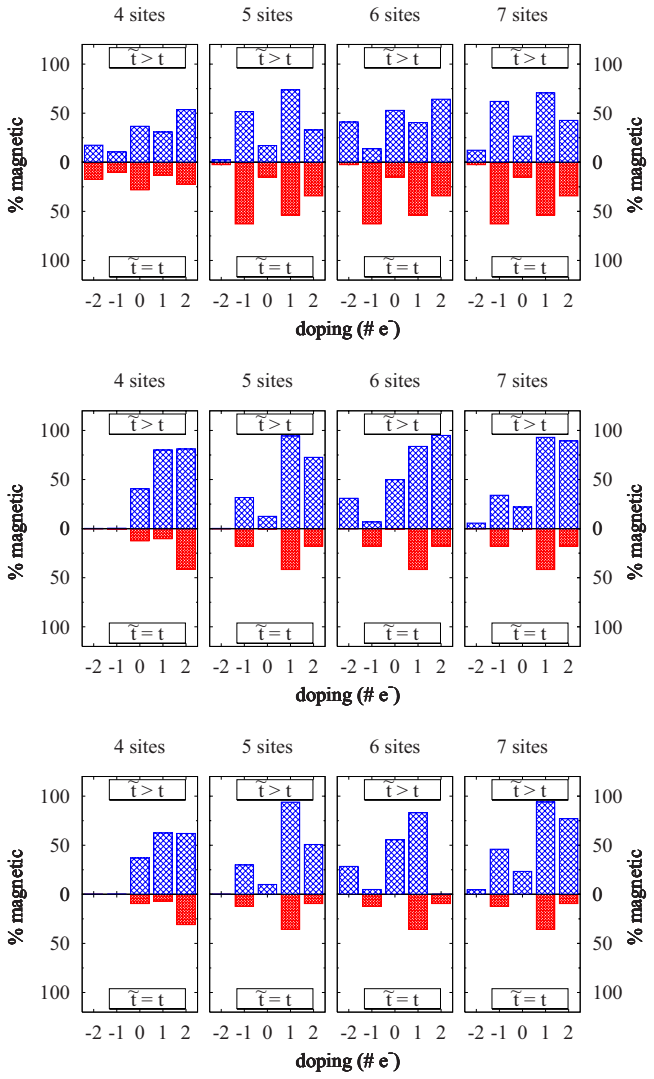

FIG. 15. (Color online) Percentage of magnetic clusters (spin 1 or greater) in an ensemble of 2D random clusters with fixed size and density, and *open boundary conditions*, as a function of electron-doping (negative=hole doping). The lower half of plots are the result of setting $\tilde{t}_{ij}=t_{ij}$, determined by the bandwidth of the lower Hubbard band. The upper half use $\tilde{t}_{ij}$ determined by the bandwidth of the upper Hubbard (D^-) band.

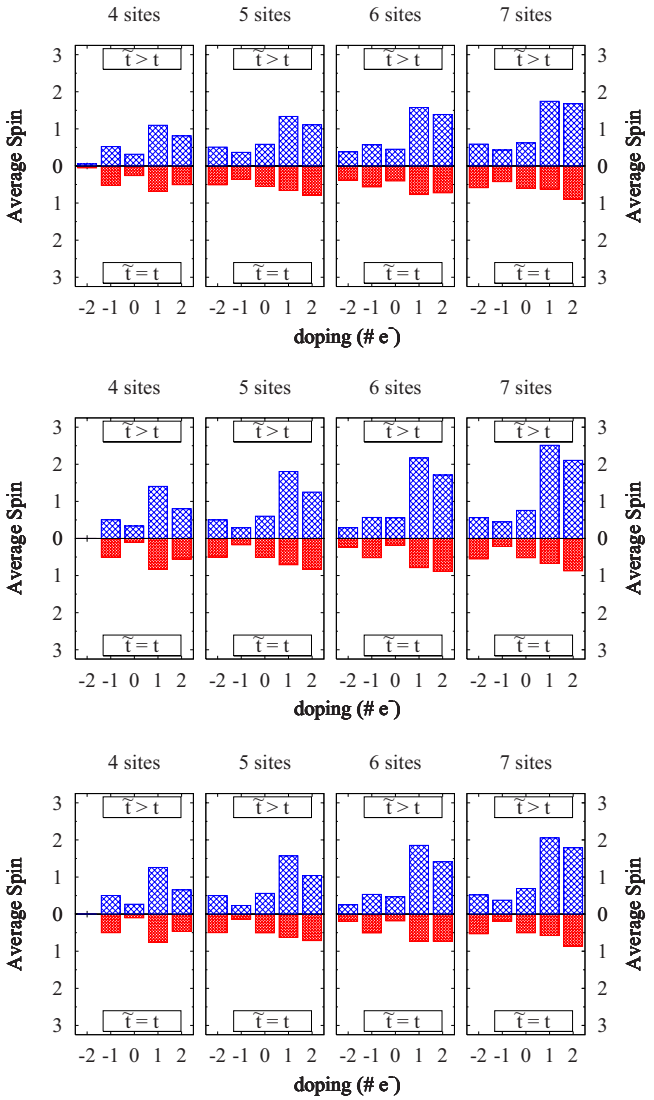

FIG. 16. (Color online) Ground-state average spin of 3D random clusters with fixed size and density, and *open boundary conditions*, as a function of electron-doping (negative=hole-doping). The lower half of plots are the result of setting $\tilde{t}_{ij}=t_{ij}$, determined by the bandwidth of the lower Hubbard band. The upper half use $\tilde{t}_{ij}$ determined by the bandwidth of the upper Hubbard (D^-) band.

ters will be connected to other clusters of different local densities. Thus, the physical situation will be intermediate between the cases of open (where each cluster is surrounded by no others) and periodic (where each cluster is effectively surrounded by others of the same density) boundary conditions. The latter is closer to the actual case at high densities, the former at low density.

We summarize the data by plotting the average spin in Figs. 14 and 16 as a function of doping (zero doping=half-filled) in two and three dimensions, respectively. These figures contrast the method of constructing clusters described above [with $\tilde{t}(r)$ and $t(r)$] with the case when both $\tilde{t}_{ij}$ and t_{ij} are equal, given by $t(|\vec{r}_i-\vec{r}_j|)$ (i.e., when the doubly occupied state is no larger than the singly occupied state). We also examine a second measure of magnetic behavior: the percentage of clusters in a given system with above minimal spin. We define any cluster with greater than minimal ground state spin (equivalently, spin ≥ 1 since the minimal spin is either 0 or 1/2) as a *magnetic cluster*, and plot the percentage of magnetic clusters vs. doping in Figs. 15 and 17 for 2D and 3D systems (with open boundary conditions), respectively.

Figures 14–17 reveal several trends which are analyzed in detail in Ref. 5. We focus on the most striking of these, which is the contrast between electron-doped and hole-doped clusters. Compared to the case where both t_{ij} and $\tilde{t}_{ij}$ are computed from the lower impurity band ($\tilde{t}=t$), when $\tilde{t}_{ij}$ is instead computed from the upper impurity band, the clusters with one extra electron have a spin distribution shifted to substantially higher spin values than those with one less electron. This effect is expected, since in our model an extra electron hops with amplitudes $\tilde{t}_{ij}$ while an extra hole hops with am-

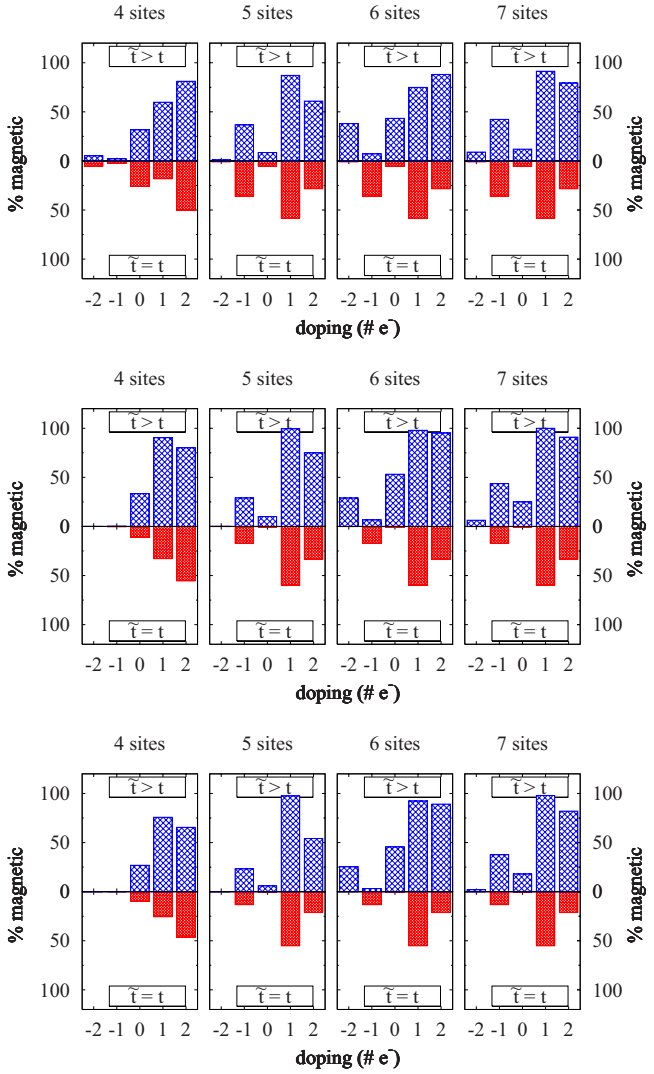

FIG. 17. (Color online) Percentage of magnetic clusters (spin 1 or greater) in an ensemble of 3D random clusters with fixed size and density, and *open boundary conditions*, as a function of electron-doping (negative=hole doping). The lower half of plots are the result of setting $\tilde{t}_{ij}=t_{ij}$, determined by the bandwidth of the lower Hubbard band. The upper half use $\tilde{t}_{ij}$ determined by the bandwidth of the upper Hubbard (D^-) band.

plitudes t_{ij}. Recall that the motivation for the model comes from the special properties of the hydrogen atom which result in mobile electrons having spatially larger wave functions than mobile holes. These cluster results show that even in strongly disordered systems a Nagaoka-type ferromagnetism can emerge at least on the nanoscale and one of the ideal conditions for this FM is an electron-doped system. Compared to those below half-filling, systems above half-filling also hold greater promise for spin polarization on longer length scales, since this would most likely arise from many aligned high-spin clusters. Additionally, we find the effect is most pronounced at the intermediate density in both 2D and 3D. This suggests that there is an optimal density for seeing Nagaoka ferromagnetism in these electron-doped regimes which is an order of magnitude lower than the Mott density.

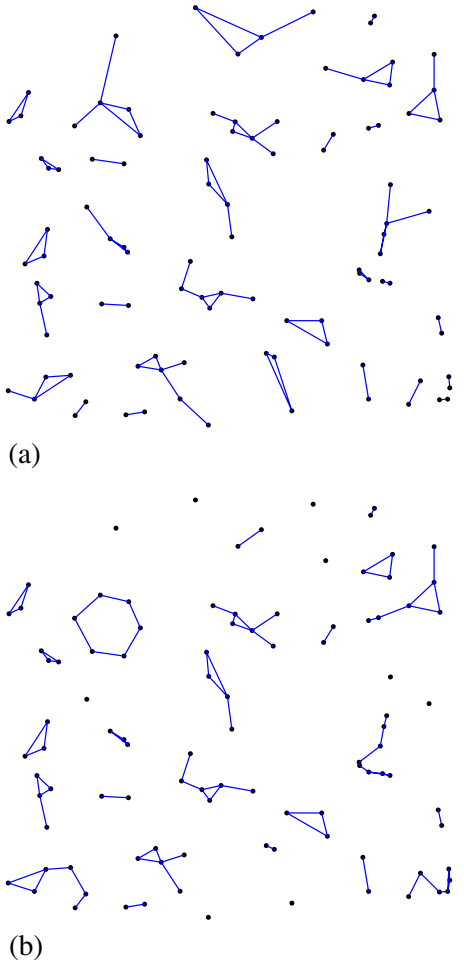

FIG. 18. (Color online) Example of decomposing a 100-site system into clusters. Part (a) uses the nearest-neighbor method and part (b) the threshold method (both described in the text). Lines (blue online) link points in the same clusters (not all hopping links between the points are shown).

V. CLUSTER ANALYSIS OF LARGE SYSTEMS

We next turn to the possibility of ferromagnetism in macroscopic samples. Our results on clusters show that high spin states (nanoscale ferromagnetism) are most abundant away from the half-filled case with electron doping. Such a situation with electron density larger than dopant density cannot be achieved in bulk systems; however it is possible to realize it in 2D heterostructures. Consequently, we limit our study of large samples to 2D, though similar results would be expected for 3D systems with finite thickness. Our strategy here is to consider a large system of Poisson-distributed random sites and divide it into clusters that can be approximately treated as independent as far as the Hubbard part of the Hamiltonian is concerned. Choice of the number of carriers in each cluster involves long-range Coulomb forces and is treated in a classical approximation described later. We solve the clusters individually using $\tilde{t}_{ij}$ and t_{ij} parameters from the band calculation, and then analyze the resulting distribution of their ground state spins. The analysis of Sec. IV D characterized random clusters with a fixed density; here

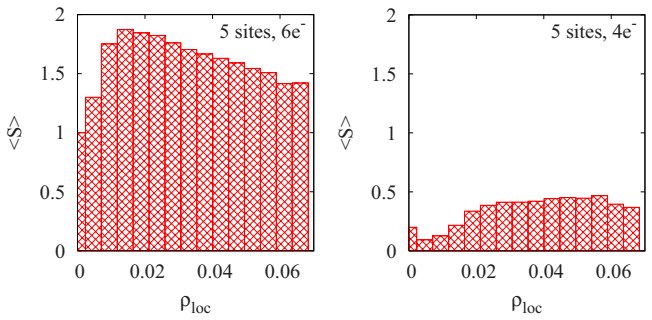

FIG. 19. (Color online) Average ground state spin vs. local density of 2D 5-site clusters. The pertinent range of local densities is divided into bins, and bar heights indicate the average ground state spin of the 5-site clusters whose density falls within the corresponding density bin. This data is from $\bar{\rho}=\frac{1}{160}$ clusters but the behavior is typical (see text).

the average density of the large system is fixed while the local density of individual clusters varies according to the Poisson distribution.

Decomposition into clusters

We begin with a set of N_{sys} randomly positioned points with some average density $\bar{\rho}$ where N_{sys} is typically 10 000–1 000 000. We then divide the points into approximately isolated clusters, solve the cluster generalized Hubbard Hamiltonian exactly, and consider their ground state statistics. We choose to divide the large set of points into clusters using a simple algorithm that proceeds as follows: (1) initially each point is a single cluster and all points are "unused." (2) Choose any unused point p and find its nearest neighbor q. (3) Merge the cluster containing p with the cluster containing q. (4) Set point p to "used" status. (5) Repeat at step 2 until no unused points remain.

In this way we form the smallest clusters such that each point belongs to the same cluster as its nearest neighbor (i.e., the point most strongly coupled to it). Note also that the minimum cluster size is 2. The advantage of this "nearest-neighbor" method is that it always keeps nearest-neighbor points in the same cluster, which is desirable from a perturbation theory standpoint. It does not, however, guarantee that the clusters include all the hopping amplitudes of the original system above some threshold. We show in Fig. 18(a) the decomposition of a 2D system into clusters using the algorithm. A weakness of the nearest neighbor method is that it will form separate clusters of strongly coupled pairs even when they are nearby other clusters and it is clearly seen from Fig. 18(a) that some of the neglected bonds are stronger than other bonds that are kept. On the same set of random sites, the result of an alternate algorithm that keeps all hopping amplitudes greater than a certain threshold (chosen so that the size of the clusters is not too large) is shown in Fig. 18(b). This technique removes the problem of isolating strongly coupled pairs/triangles from other nearby sites but it has the disadvantage of being very sensitive to the threshold, adding another degree of arbitrariness. We find that both methods give reasonable decompositions into clusters and

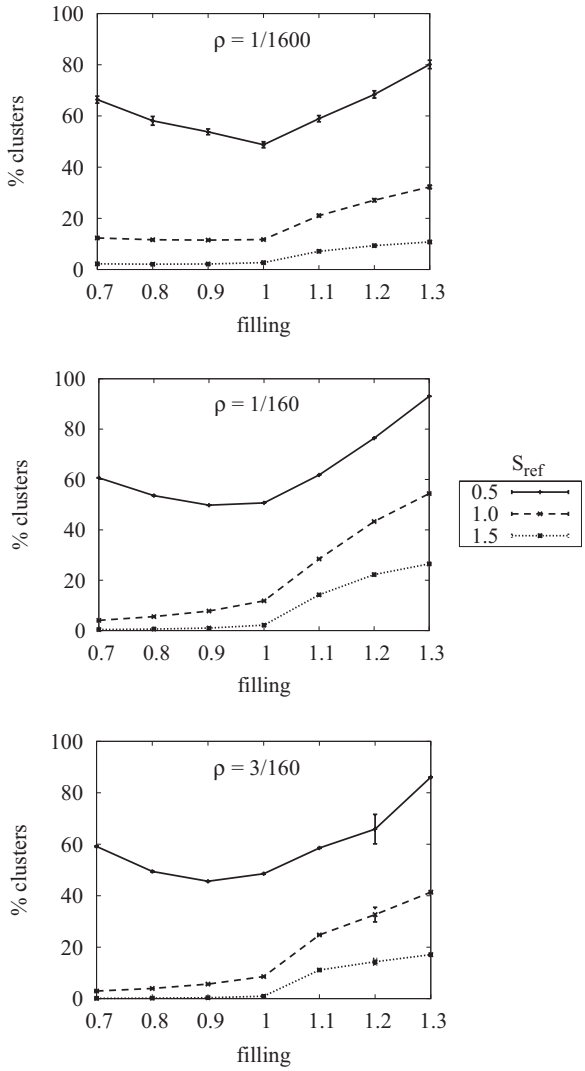

FIG. 20. Percentage of clusters with total spin greater than the reference value S_{ref}, specified in the key, as a function of filling (1.0=half-filling). Plots correspond to densities $\rho=\frac{1}{1600}$, $\frac{1}{160}$, and $\frac{3}{160}$ as indicated in their titles.

the choice of algorithm not unique. In this work, we use the nearest-neighbor method outlined above, and leave a more detailed assessment and comparison of clustering methods for later work.

We diagonalize all the cluster Hamiltonians individually and compile the resulting data to arrive at the distribution of spin values from the ensemble of clusters (obtained from many different large system realizations). In this case, there is substantial fluctuation in the local density of clusters. Even the mean local density for clusters of different size is different; only the average density of the *entire* system is fixed. The results, however, show the same general trends as the clusters with fixed local density described earlier. For a direct comparison see Ref. 5.

We also find that there is a weak correlation between local density (ρ_{loc}) and average ground state spin $\langle S\rangle$. We observe quite generally that 2D clusters with one extra electron ($N_e=N_s+1$) have a peak in $\langle S\rangle$ near $\rho_{\text{loc}}\approx 0.015$ while those with one hole ($N_e=N_s-1$) have relatively smaller values of $\langle S\rangle$

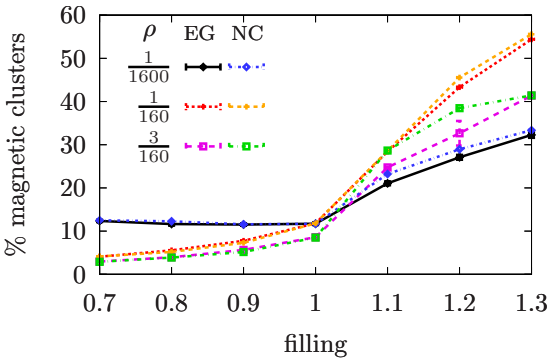

FIG. 21. (Color online) Comparison of the percentage of magnetic clusters (those with greater than minimal ground state spin) when Coulomb interactions are ignored or accounted for using a generalized Coulomb glass analysis. The plot shows, for densities $\rho=\frac{1}{1600}$, $\frac{1}{160}$, and $\frac{3}{160}$, percentages of the no-Coulomb case and electron glass.

that are less sensitive to changes in ρ_{loc}. Figure 19 shows this typical behavior for 5-site clusters with $\bar{\rho}=\frac{1}{160}$ and $N_e=N_s\pm 1$. Similar qualitative behavior is found for other clusters sizes $4\leq N_s\leq 7$ from systems with $\bar{\rho}=\frac{1}{1600},\frac{3}{160}$, though $\langle S\rangle$ tends to be higher for larger size clusters. The location of the peak at $\rho_{\mathrm{loc}}\approx 0.015$ is important to our consideration of different large-system densities $\bar{\rho}$, since we find that clusters with $\rho_{\mathrm{loc}}/\bar{\rho}\in[2,4]$ are most prevalent. In the case $\bar{\rho}=\frac{1}{160}=0.00625$, $\rho_{\mathrm{loc}}=0.015$ corresponds to $\rho_{\mathrm{loc}}/\bar{\rho}=2.4$, whereas for $\bar{\rho}=\frac{1}{1600}=0.000625$ and $\bar{\rho}=\frac{3}{160}=0.01875$ the corresponding values of $\rho_{\mathrm{loc}}/\bar{\rho}$ are 24 and 0.8, respectively. This suggests that the $\bar{\rho}=\frac{1}{160}$ case will show the greatest overall magnetism, an inference that was seen in the fixed density clusters of Sec. IV D.

We next consider the spin distribution of a large system with a fixed number of sites N_{sys} and doping (fixed total electron number N_e^{tot}). The system is partitioned into clusters of size $N_s=2-7$, which are treated as being independent. It only remains to determine how the electrons will be distributed among the clusters—after the number of electrons on each cluster is known, the clusters can be independently solved and their ground-state spin tabulated. We calculate the electron distribution using a method which takes into account Coulomb interactions via a classical approximation. As stated before, we consider *only* 2D systems since our interest is primarily in 2D heterostructures. Including Coulomb interactions is particularly relevant for low-density insulating systems where the interactions between charged centers (or clusters) are not screened effectively, and have a slow $(1/r)$ fall-off as shown by Efros and Shklovskii (ES).[78]

We begin by solving each cluster for range of total electrons near half-filling and then determine the minimum energy electron distribution by solving a generalized electron glass problem analogous to the ES model for individual sites[78–81] but involving different charge states of each *cluster*. Such a treatment finds the ground state of the many-body system, accounting for the differences in ground-state energy of the clusters *and* the Coulomb energy between charged clusters. Details are provided in Ref. 5.

Once we have determined the distribution of electrons among the many clusters of the large system, we compute the percentage of clusters with spin greater than a given reference spin S_{ref}. This quantity is averaged over many random realizations of the large cluster system. The (ensemble-averaged) percentage of clusters with spin $\geq S_{ref}$ for $S_{ref}=\frac{1}{2}$, 1, and $\frac{3}{2}$ is shown in Fig. 20 for our standard densities $\rho=\frac{1}{1600}$, $\frac{1}{160}$, and $\frac{3}{160}$. For $S_{ref}=1$, these percentages correspond to our earlier definition of "magnetic clusters," and Fig. 21 compares the results to the same calculation but ignoring Coulomb interactions. We see that Coulomb interactions slightly deplete the number of high-spin clusters, particularly in the electron-doped case. Figure 21 also shows that even in the presence of long-range Coulomb interactions there is a sizable percentage of magnetic clusters at modest electron doping. In a strictly 2D system, in order for the magnetic clusters to percolate they must account for 50% of the system, which is only attained at large filling factors ($\approx$1.2 in the best case of $\rho=\frac{1}{160}$).[82] In 3D, however, the percolation threshold is much lower, so a parallel calculation in a 3D or thick 2D system (which behaves as a 3D system on short length scales) should yield even more promising results. As the impurity density is increased at fixed doping the average percentage of magnetic clusters has a nonmonotonic behavior. There is an optimal impurity density (nearest to $\rho=\frac{1}{160}$ in our data) that results in an on-average maximal percentage of magnetic clusters, just as we saw in the case of random finite clusters of fixed density in Sec. IV D. Altogether, the presence of many high-spin clusters provides a necessary ingredient for ferromagnetism on mesoscopic and possibly even macroscopic length scales.

VI. CONCLUSIONS

We have formulated a generalized Hubbard model with three parameters (t, $\tilde{t}$, and U), appropriate for doped semiconductors, which has an occupation-dependent hopping term and therefore intrinsic electron-hole asymmetry characteristic of the hydrogenic center. This generalized disordered Hubbard model is numerically solved using exact diagonalization on 2D finite lattices, selected symmetric clusters, and completely random clusters. We then explore the possibility of ferromagnetism in large size systems of doped semiconductors, primarily for dopant densities below the Mott density, by combining our exact results on clusters with a many-body version of the electron glass model to take into account long range Coulomb interactions. Our work represents the most extensive study to-date of the magnetic phase diagram of conventional doped semiconductors on both sides of the uncompensated system—with hole doping (as in compensated semiconductors), *as well as* (the heretofore unstudied) electron doping.

Our results on finite (periodic) lattices, as well as selected clusters and distorted/randomized versions of them, show that high-spin ground states generally occur at large U/t (low-impurity density). On a bipartite lattice one carrier away from half-filling, Nagaoka's theorem guarantees a maximal spin state in the limit $U/t\rightarrow\infty$. In the finite lattices that satisfy Nagaoka's theorem, we find maximal spin states at large but finite U/t. In clusters (with less symmetry than a lattice), high-spin ground states are found to be quite sensi-

tive to the cluster geometry, though they all exist at large U/t.

Most importantly, we find that the properties of the hydrogen atom give rise to a crucial difference in systems with shallow hydrogenic dopants between the electron doping and hole doping away from the half-filled (uncompensated) system. In lattices as well as clusters we see a greatly enhanced occurrence of spin polarization in electron-doped (above half-filling) systems. In systems above half-filling we also find that increasing $\tilde{t}/t$ can significantly increase the likelihood of this nanoscale ferromagnetism. These results confirm our expectation that the greater the spatial extent of a doubly occupied site's wave function (relative to the wave function of a singly-occupied site), the more favorable spin polarization becomes.

The analysis of ground-state spin behavior in completely random clusters reveals many of the same conclusions we found for the selected symmetric clusters. Namely, we again find that electron doping and a larger $\tilde{t}/t$ favor spin polarization. The electron-hole asymmetry found in all of the random ensembles implies that in real semiconductor systems there is a significant difference between doping above and below half-filling. Spin polarization is much more prevalent in systems above half-filling, an effect which we again emphasize as arising from the physical properties of the dopant atom. Unlike in the case of selected clusters, where ferromagnetism is generally more prevalent at larger U/t, we find that within the low-density range considered (well below the metal-insulator transition), there is an optimal density for finding high-spin (random) clusters. This interesting observation is likely due to clusters breaking up into separate, effectively disconnected, pieces at very low densities, which hinders carrier movement and thereby the alignment of spins in the ground state. We also study the problem of distributing electrons onto the cluster components of a large system, where we find that Coulomb interactions *decrease* the number of clusters with above minimal spin but only slightly. In such systems we find a sizeable percentage of high spin clusters, suggesting that Nagaoka type ferromagnetism is a possibility in this electron doped region at densities about an order of magnitude below the Mott density. Taking all these results together, we expect high spin clusters to be observable in systems with a low density (large Hubbard U/t) of centers and a small *excess* of electrons. The latter requirement is difficult to realize in 3D bulk systems but could be met in doped quantum dots and 2D heterostructures. For example, doped quantum dots with dopant number $N_d=6-15$ and a small excess of electrons $N_e-N_d=1-2$ would be ideal systems for finding high-spin ground states. Also, in modulated structures with dopants in both quantum wells and barrier regions, regions of excess electrons can be achieved in the quantum wells, unlike in true bulk doped semiconductors. We also note that the artificial cluster geometries studied in Sec. IV B have real world applications through recently developed technology which allows precise placement of phosphorous donors in silicon.[83]

ACKNOWLEDGMENTS

This research was supported by NSF-MRSEC, Grants No. DMR-0213706 and No. DMR-0819860. R.N.B. acknowledges the hospitality of the Aspen Center for Physics, where some of the work was written up. The writing of this work was partially supported by the Laboratory Directed Research and Development program at Sandia National Laboratories (E.N.). Sandia is a multiprogram laboratory operated by Sandia Corporation, a Lockheed Martin Co., for the United States Department of Energy's National Nuclear Security Administration under Contract No. DE-AC04-94AL85000.

[1] P. W. Anderson, *Concepts in Solids* (Benjamin, Reading, MA, 1963).
[2] D. E. Angelescu and R. N. Bhatt, Phys. Rev. B **65**, 075211 (2002).
[3] Y. Nagaoka, Phys. Rev. **147**, 392 (1966).
[4] J. E. Hirsch, Phys. Rev. B **31**, 4403 (1985).
[5] E. Nielsen, Ph.D. thesis, Princeton University, 2008.
[6] M. J. Hirsch, D. F. Holcomb, R. N. Bhatt, and M. A. Paalanen, Phys. Rev. Lett. **68**, 1418 (1992).
[7] R. N. Bhatt and P. A. Lee, Phys. Rev. Lett. **48**, 344 (1982).
[8] H. Ohno, Science **281**, 951 (1998).
[9] D. Chiba, K. Takamura, F. Matsukura, and H. Ohno, Appl. Phys. Lett. **82**, 3020 (2003).
[10] M. Berciu and R. N. Bhatt, Phys. Rev. Lett. **87**, 107203 (2001).
[11] M. P. Kennett, M. Berciu, and R. N. Bhatt, Phys. Rev. B **66**, 045207 (2002).
[12] G. A. Thomas, M. Capizzi, F. DeRosa, R. N. Bhatt, and T. M. Rice, Phys. Rev. B **23**, 5472 (1981).
[13] K. Andres, R. N. Bhatt, P. Goalwin, T. M. Rice, and R. E. Walstedt, Phys. Rev. B **24**, 244 (1981).
[14] C. L. Pekeris, Phys. Rev. **126**, 1470 (1962).
[15] N. F. Mott, *Metal-insulator Transitions*, 2nd ed. (Taylor & Francis, London, 1990) and references therein.
[16] H. A. Bethe and E. E. Salpeter, *Quantum Mechanics of 1 and 2 Electron Atoms* (Springer, New York, 1977).
[17] R. N. Bhatt and T. M. Rice, Phys. Rev. B **23**, 1920 (1981).
[18] E. Eisenberg, R. A. Berkovits, D. A. Huse, and B. L. Altshuler, Phys. Rev. B **65**, 134437 (2002).
[19] E. Nielsen and R. N. Bhatt, Phys. Rev. B **76**, 161202(R) (2007).
[20] J. Hubbard, Proc. R. Soc. London, Ser. A **276**, 238 (1963).
[21] M. C. Gutzwiller, Phys. Rev. Lett. **10**, 159 (1963).
[22] J. Kanamori, Prog. Theor. Phys. **30**, 275 (1963).
[23] P. W. Anderson, Solid State Phys. **14**, 99 (1963).
[24] S. Pyo, L. Ma, J. He, Q. Xu, and Y. Yang, J. Appl. Phys. **98**, 054303 (2005).
[25] D. B. McWhan, A. Menth, J. P. Remeika, W. F. Brinkman, and T. M. Rice, Phys. Rev. B **7**, 1920 (1973).
[26] S. A. Carter, J. Yang, T. F. Rosenbaum, J. Spalek, and J. M. Honig, Phys. Rev. B **43**, 607 (1991).
[27] S. Ogawa, J. Appl. Phys. **50**, 2308 (1979).
[28] T. Thio and J. W. Bennett, Phys. Rev. B **50**, 10574 (1994).
[29] T. Thio, J. W. Bennett, and T. R. Thurston, Phys. Rev. B **52**,

3555 (1995).
[30] J. Wu, L. Ma, and Y. Yang, Phys. Rev. B **69**, 115321 (2004).
[31] M. Sing, U. Schwingenschlögl, R. Claessen, P. Blaha, J. M. P. Carmelo, L. M. Martelo, P. D. Sacramento, M. Dressel, and C. S. Jacobsen, Phys. Rev. B **68**, 125111 (2003).
[32] P. W. Anderson, Science **235**, 1196 (1987).
[33] P. A. Lee, N. Nagaosa, and X.-G. Wen, Rev. Mod. Phys. **78**, 17 (2006).
[34] Y. A. Izyumov, Phys. Usp. **40**, 445 (1997).
[35] A. Macridin, M. Jarrell, T. Maier, and G. A. Sawatzky, Phys. Rev. B **71**, 134527 (2005).
[36] A. Ferreira da Silva, R. Kishore, and I. C. da Cunha Lima, Phys. Rev. B **23**, 4035 (1981).
[37] M. C. Refolio, J. M. López Sancho, M. P. López Sancho, and J. Rubio, Phys. Rev. B **53**, 4791 (1996).
[38] M. Rontani, F. Rossi, F. Manghi, and E. Molinari, Phys. Rev. B **59**, 10165 (1999).
[39] T. Hanisch, G. S. Uhrig, and E. Müller-Hartmann, Phys. Rev. B **56**, 13960 (1997).
[40] T. Wegner, M. Potthoff, and W. Nolting, Phys. Rev. B **57**, 6211 (1998).
[41] K. Penc, H. Shiba, F. Mila, and T. Tsukagoshi, Phys. Rev. B **54**, 4056 (1996).
[42] R. Frésard and G. Kotliar, Phys. Rev. B **56**, 12909 (1997).
[43] J. Kuei and R. T. Scalettar, Phys. Rev. B **55**, 14968 (1997).
[44] K. Byczuk, M. Ulmke, and D. Vollhardt, Phys. Rev. Lett. **90**, 196403 (2003).
[45] F. Becca and S. Sorella, Phys. Rev. Lett. **86**, 3396 (2001).
[46] T. Obermeier, T. Pruschke, and J. Keller, Phys. Rev. B **56**, R8479 (1997).
[47] D. Jaksch and P. Zoller, Ann. Phys. **315**, 52 (2005).
[48] R. N. Bhatt, Phys. Rev. B **24**, 3630 (1981).
[49] K. A. Chao, J. Spalek, and A. M. Olés, J. Phys. C **10**, L271 (1977).
[50] K. A. Chao, J. Spalek, and A. M. Olés, Phys. Rev. B **18**, 3453 (1978).
[51] W. F. Brinkman and T. M. Rice, Phys. Rev. B **2**, 1324 (1970).
[52] B. I. Shraiman and E. D. Siggia, Phys. Rev. Lett. **61**, 467 (1988).
[53] H. Tasaki, Commun. Math. Phys. **242**, 445 (2003).
[54] G.-S. Tian, J. Phys. A **23**, 2231 (1990).
[55] H. Tasaki, Prog. Theor. Phys. **99**, 489 (1998).
[56] W. Sasaki and J. Kinoshita, J. Phys. Soc. Jpn. **25**, 1622 (1968).
[57] W. Sasaki, J. Phys. (Paris), Colloq. **37**, C4-311 (1976).
[58] H. Ue and S. Maekawa, Phys. Rev. B **3**, 4232 (1971).
[59] J. D. Quirt and J. R. Marko, Phys. Rev. B **7**, 3842 (1973).
[60] R. N. Bhatt, *Proceedings of the 20th International Conference on Physics of Semiconductors* (World Scientific, Singapore, 1990), p. 2633.
[61] R. N. Bhatt, M. A. Paalanen, and S. Sachdev, J. Phys. Colloq. **49**, C8-1179 (1988).
[62] D. S. Fisher, Phys. Rev. B **50**, 3799 (1994).
[63] D. Holcomb, in *Localisation and Interactions in Disordered Metals and Doped Semiconductors: Proceedings of the 31st Scottish Universities Summer School in Physics*, edited by D. M. Finlayson (SUSSP, Edinburgh, 1986) p. 313.
[64] M. A. Paalanen, J. E. Graebner, R. N. Bhatt, and S. Sachdev, Phys. Rev. Lett. **61**, 597 (1988).
[65] S. Narita and M. Taniguchi, Phys. Rev. Lett. **36**, 913 (1976).
[66] P. Norton, Phys. Rev. Lett. **37**, 164 (1976).
[67] M. Taniguchi and S. Narita, J. Phys. Soc. Jpn. **43**, 1262 (1977).
[68] E. Nielsen and R. N. Bhatt (unpublished).
[69] M. Capizzi, G. A. Thomas, F. DeRosa, R. N. Bhatt, and T. M. Rice, Solid State Commun. **31**, 611 (1979).
[70] C. Herring and M. Flicker, Phys. Rev. **134**, A362 (1964).
[71] E. Fradkin, *Field Theories of Condensed Matter Systems* (Westview Press, 1991).
[72] H. Q. Lin and J. E. Hirsch, Phys. Rev. B **52**, 16155 (1995).
[73] N. M. R. Peres, M. A. N. Araújo, and D. Bozi, Phys. Rev. B **70**, 195122 (2004).
[74] S. Ghosh and A. Singh, Phys. Rev. B **77**, 094430 (2008).
[75] G. M. Pastor, R. Hirsch, and B. Mühlschlegel, Phys. Rev. Lett. **72**, 3879 (1994).
[76] J. O. Haerter and B. S. Shastry, Phys. Rev. Lett. **95**, 087202 (2005).
[77] G. M. Pastor, R. Hirsch, and B. Mühlschlegel, Phys. Rev. B **53**, 10382 (1996).
[78] A. L. Efros and B. I. Shklovskii, J. Phys. C **8**, L49 (1975).
[79] A. L. Efros, J. Phys. C **9**, 2021 (1976).
[80] J. H. Davies, P. A. Lee, and T. M. Rice, Phys. Rev. Lett. **49**, 758 (1982).
[81] J. H. Davies, P. A. Lee, and T. M. Rice, Phys. Rev. B **29**, 4260 (1984).
[82] One cautionary remark is that for *large* deviations from half-filling, the model must be augmented by an on-site disorder term due to the random fields of the charged centers, which could modify the spin polarization.
[83] S. R. Schofield, N. J. Curson, M. Y. Simmons, F. J. Ruess, T. Hallam, L. Oberbeck, and R. G. Clark, Phys. Rev. Lett. **91**, 136104 (2003).